12A.7 AN OBSERVATIONAL STUDY OF ATMOSPHERIC BORE FORMATION FROM COLLIDING DENSITY CURRENTS

David E. Kingsmill [*1] and N. Andrew Crook[2]

[1]Desert Research Institute, Reno, Nevada
[2]National Center for Atmospheric Research, Boulder, Colorado

1. INTRODUCTION

Boundary layer convergence zones (or boundaries) are well known factors in the initiation of deep convection and the modulation of its evolution. Gust fronts, sea-breeze fronts, cold fronts and drylines are examples of such phenomena. Structural investigations of these boundaries indicate that they are often dynamically similar to density currents (Simpson 1997). This class of hydrodynamic phenomena is characterized by its mass transport behavior, with the denser fluid traveling at least as fast as the leading edge of the density current. Internal bores are another closely related class of hydrodynamic flows. The most fundamental difference between these two phenomena is that bores, at least in their purest form, act like gravity waves, and are void of mass transport character. This implies that fluid flows through a bore rather than collecting behind it.

The most commonly documented scenario for bore formation involves a density current propagating into a region with strong static stability, such as a nocturnal inversion. Another mechanism for bore generation is from the collision of two density currents. Clarke (1983) and Smith (1986) are among the first observational studies to propose this hypothesis. Wakimoto and Kingsmill (1995) were the first to observationally document the detailed evolution and three-dimensional structure of a bore resulting from colliding density currents. An important unresolved question is why some density current collisions produce bores while others do not. To address this issue, ten cases involving collisions of boundaries exhibiting density current behavior are analyzed using data collected from the Convection and Precipitation/Electrification (CaPE) project conducted in east-central Florida during the summer of 1991 (Wakimoto and Lew 1993).

2. DATA SOURCES AND CASE SELECTION

The CaPE experiment operated in east central Florida near Cape Canaveral during July and August 1991. A broad array of observing platforms was deployed such as Doppler and polarimetric radars, research aircraft, meteorological towers, sounding systems, mesonet stations and cameras for cloud photography. For this study, a subset of these platforms was employed. The National Center for Atmospheric Research (NCAR) CP3 and CP4 Doppler radars (C-band) and the Federal Aviation Administration sponsored FL2 and UND Doppler radars (C-band) were used to document boundary structure and propagation, initiation of convection, and air motions. Thermodynamic information was obtained from two sources. Atmospheric soundings were performed by three (two fixed and one mobile) Cross-chain Loran Atmospheric Sounding Systems (CLASS) operated by NCAR and by two non-CLASS sounding systems at Orlando and Cape Canaveral. Complementary 1-min surface observations were obtained from the second generation NCAR Portable Automated.

A total of ten boundary collision events were identified in perusing the Doppler radar data from CaPE. All of these cases involved a gust front (GF) from the western half of the CaPE domain and a sea-breeze front (SBF) from the East Coast of the Florida peninsula. A few of the SBF's were modified slightly by outflows from storms that were earlier initiated on or behind the SBF. Similar to the West Coast fronts described by Wilson and Megenhardt (1997), most of the GF's could be traced back to the western coast of the Florida peninsula, originating from storms forming on the west coast sea-breeze front

3. STRUCTURE AND EVOLUTION

There have been several detailed case studies describing the structure and evolution of boundary collisions utilizing the CaPE dataset, but only the 12 August case of Wakimoto and Kingsmill (1995) focused on post-collision boundary layer structure. However, in examining the other cases, it was discovered that similar boundary layer structures were often apparent after the collisions. The case on 2 August is used here to illustrate the fundamental aspects of these structures (Figs. 1 and 2).

At 2222 UTC (Fig. 1a), a gust front and a sea-breeze front are located about 25 km west-northwest of CP4. The gust front propagating toward 115° is ~5 km west-northwest of the sea-breeze front propagating toward 285°. These boundaries collide 8 minutes later at 2230 UTC. Several minutes after the collision at 2237 UTC (Fig. 1b), two distinct convergence boundaries are evident in the radial velocity field. Proceeding outbound from CP4 along the 295° radial, velocities are first +6 to +7 m s^{-1} (positive is outbound) then transition to weakly negative (-1 to -2 m s^{-1}), implying a radial convergence. A little further downrange the radial velocities become weakly positive (+1 to +2 m s^{-1}) then transition to moderately negative (-4 to –5 m s^{-1}), implying another zone of radial convergence. Seventeen minutes later at 2254 UTC (Fig. 1c), these post-collision convergence boundaries have amplified and propagated. They are also evident as two distinct thin lines of enhanced reflectivity between 10-20 dBZ_e. The boundary closer to CP4 has

*Corresponding author address: David E. Kingsmill, Desert Research Institute, 2215 Raggio Parkway, Reno, NV 89512-1095; email: davidk@dri.edu

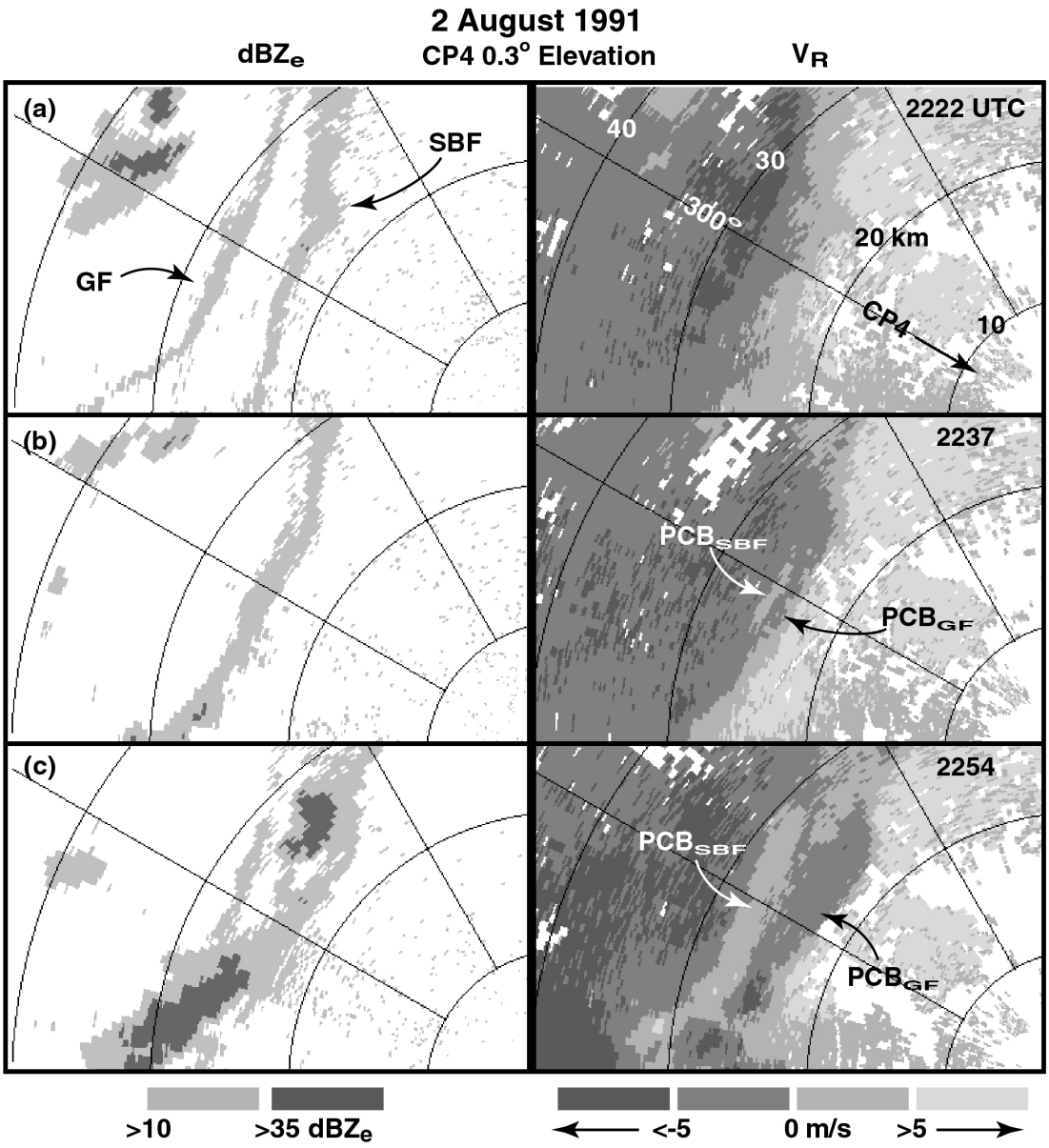

Figure 1. CP4 radar reflectivity (left) and radial velocity (right) at 0.3° elevation angle on 2 August 1991 (a) 2222 UTC, (b) 2237 UTC and (c) 2254 UTC. Radar reflectivity in dBZ_e and radial velocity in m s^{-1}, with grey scales at bottom of figure. Plotted sector is northwest of CP4 with range rings at 10 km intervals.

moved closer and in a direction similar to the propagation direction of the pre-collision gust front. As a means of identification, this boundary is defined as the gust front post-collision boundary (PCB_{GF}). Likewise, the boundary more distant from CP4 has moved further away and in a direction similar to the propagation direction of the pre-collision sea-breeze front. This boundary is therefore defined as the sea-breeze front post-collision boundary (PCB_{SBF}). PCB_{GF} and PCB_{SBF} continue to propagate away from each other over the next 15 minutes and appear to modulate the convection initiated just after the collision. Color animations of this and other boundary collision events from this study can be viewed at www.dri.edu/Projects/Radar/Collision.html

The propagation characteristics of these boundaries evolve through three regimes (Fig. 2). Prior to the collision at 2230 UTC, the slopes of the gust front and sea-breeze front curves indicate that they are moving at about 4 m s^{-1}, with some evidence of slowing immediately before the collision. After the collision, until about 2253 UTC, the post-collision boundaries propagate at a significantly slower rate than their pre-collision progenitors. Thereafter, their propagation speeds increase, apparently in response to outflows generated by convection initiated from the collision and modulated by the post-collision boundaries.

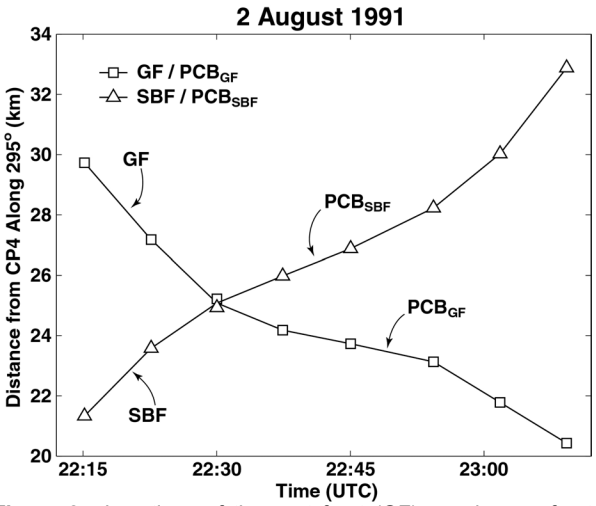

Figure 2. Locations of the gust front (GF), sea-breeze front (SBF), gust front post-collision boundary (PCB_{GF}) and sea-breeze front post-collision boundary (PCB_{SBF}) along the CP4 295° radial during the period 2215-2309 UTC on 2 August 1991.

3.1 Pre-collision characteristics

A survey of all ten cases indicates that gust fronts propagated on average toward the east at 8.0 m s^{-1}. Their propagation directions varied between north-northeast and southeast while their speeds mainly varied between 4.5 and 10.0 m s^{-1}, with an extreme value of 17.0 m s^{-1} on 15 July. In contrast, average sea-breeze front propagation direction was toward the west, with much less variation than gust front propagation direction. Sea-breeze fronts also propagated more slowly than gust fronts, on average at a speed of 3.0 m s^{-1}. In fact, three cases involved stationary sea-breeze fronts.

Owing to the limited sounding coverage behind these boundaries, a kinematic approach to determining boundary depth was adopted using Doppler radar data. The results of this analysis indicate that the airmass behind gust fronts was on average 1.1 km deep, with considerable variability (0.5 to 2.5 km). The airmass behind sea-breeze fronts was on average shallower (0.7 km) and showed much less variation (0.3 to 1.1 km). However, in three cases, sea-breeze front depth exceeded gust front depth, a trend that can be attributed to sea-breeze enhancement by thunderstorm outflows.

A combination of sounding and surface mesonet data were used to define the thermodynamic character of these boundaries. The airmass behind gust fronts exhibited θ_v deficits that almost always exceeded those associated with the airmass behind the corresponding sea-breeze fronts, on average by a factor of more than two. As with other variables, the post gust front airmasses showed much greater variability in θ_v deficit compared to the post sea-breeze front airmasses.

Boundary propagation speed, depth and θ_v deficit were combined to derive Froude numbers indicating that the boundaries behaved like density currents. In addition, maximum ground-relative airflow behind and orthogonal to these boundaries is consistently larger than boundary propagations speeds, indicating that mass is being transported toward the boundary front, a fundamental property of density currents.

3.2 Post-collision characteristics

Of the ten cases, only three did not produce dual collision boundaries. These collision events produced gust front post-collision boundaries but no sea-breeze front post-collision boundaries. Interestingly, these three cases were associated with stationary sea-breeze fronts. About 70% of the post-collision boundaries initiated or expanded convection in some way, which bolsters the motivation for studying these boundary collision induced phenomena.

Unlike the pre-collision gust fronts and sea-breeze fronts, the post-collision boundaries do not show a consistent trend of mass transport toward the boundary front. Although the average behavior of gust front induced post-collision boundaries is indicative of mass transport, there are four cases where the maximum airflow behind the post-collision boundary was either less than or approximately equal to the post-collision boundary propagation speed. Sea-breeze front induced post-collision boundaries showed even less mass transport character, with average propagation speeds exceeding average maximum airflow behind the collision boundary.

Given that many of the post-collision boundaries exhibit behavior counter to that expected for density currents, an alternate classification is required. Internal bores are one class of hydrodynamic phenomena that may explain the lack of mass transport with some collision boundaries. One of the fundamental characteristics of bores is that they move faster than the low-level airflow upon which they travel (Simpson 1997). In other words, the purest form of a bore does not transport mass. Therefore, a relatively simplistic, but consistent scheme based on mass transport is used to characterize the hydrodynamic nature of observed post-collision boundaries. If maximum airflow behind the post-collision boundary was 2 m s^{-1} greater than the post-collision boundary propagation speed, the post-collision boundary was categorized as a density current. This threshold was based upon the fact that all of the pre-collision boundaries were characterized as density currents and the maximum boundary-normal airflow in their wakes was at least 2 m s^{-1} greater than their propagation speed. If mass transport was not evident from the kinematic data, the post-collision boundary was categorized as a bore. The third and final category was for those post-collision boundaries that exhibited minimal mass transport. These cases are assumed to be hybrids of the pure bore and pure density current. The results of this categorization indicate that gust front induced post-collision boundaries behaved like density currents in 6 of the 10 cases. The remaining four cases were split evenly between pure bores and hybrid bore/density currents. In contrast, the seven sea-breeze front induced post-collision boundaries showed no pure density current characteristics, most often (5 out of 7) behaving like pure bores.

Gust front induced post-collision boundaries showed a tendency to behave as bores or bore/density current hybrids when the propagation speeds of pre-collision gust fronts and sea-breeze fronts were most similar (Fig. 3a). Density currents resulted when gust front propagation speed was at least 4 m s^{-1} greater than sea-breeze front propagation speed. The trends for sea-breeze front induced post-collision boundaries were less distinct (Fig. 3b). Aside from the previously mentioned fact that stationary sea-breeze fronts did not produce post-collision boundaries, there were no clear tendencies when examining the contrast between propagation speed of gust fronts and sea-breeze fronts. Bores or bore/density current hybrids formed even when gust fronts propagated much faster than sea-breeze fronts.

4. SUMMARY AND CONCLUSIONS

This study has examined boundary layer convergence lines and the types of structures that result after their collision, such as bores. Ten cases, each involving a gust front and a sea-breeze front, were analyzed using data from the 1991 CaPE project conducted in east central Florida. The gust fronts in these collisions were on average deeper, denser and faster propagating than their sea-breeze front counterparts. Gust fronts also showed much greater variability in these parameters compared to sea-breeze fronts. Froude number calculations indicated that the gust fronts and sea-breeze fronts were dynamically similar to density currents.

Seven of the ten collision cases produced dual boundaries that moved away from each other in a relative sense. These post-collision boundaries were categorized based on their mass transport properties. Those moving in the same direction and oriented similar to the pre-collision gust front were varied in character. In six of the ten cases, they transported mass in the manner of density currents. The remaining cases involved gust front induced post-collision boundaries that exhibited little or no mass transport and were categorized as bores or bore/density current hybrids. In contrast, the seven sea-breeze front induced post-collision boundaries showed no purely density current mass transport behavior. Instead they exhibited the properties of bores or bore/density current hybrids.

For post-collision boundaries induced by gust fronts, similarity of pre-collision ground-relative propagation speed was the best indicator of bore formation (Fig 3). The comparison of these parameters was less helpful in trying to predict the development of bores induced by sea-breeze fronts. All non-stationary sea-breeze fronts produced bores or bore/density current hybrids.

ACKNOWLEDGEMENTS

The efforts of the first author (DEK) in performing this research were sponsored by the National Science Foundation under grant ATM-9901688.

REFERENCES

Clarke, R. H., 1983: Internal atmospheric bores in northern Australia. *Aust. Meteor. Mag.*, **31**, 147-160.

Simpson, J. E., 1997: *Gravity Currents: In the Environment and the Laboratory*, Cambridge University Press, 2nd Edition, 244 pp.

Smith, R. K., 1986: Evening glory wave-cloud lines in northwestern Australia. *Aust. Meteor. Mag.*, **34**, 27-33.

Wakimoto, R. M. and J. K. Lew, 1993: Observations of a Florida waterspout during CaPE. *Wea. Forecasting*, **8**, 412-423.

Wakimoto, R. M. and D. E. Kingsmill, 1995: Structure of an atmospheric undular bore generated from colliding boundaries during CaPE. *Mon. Wea. Rev.*, **123**, 1374-1393.

Wilson, J. W. and D. L. Megenhardt, 1997: Thunderstorm initiation, organization and lifetime associated with Florida boundary layer convergence lines. *Mon. Wea. Rev.*, **125**, 1507-1525.

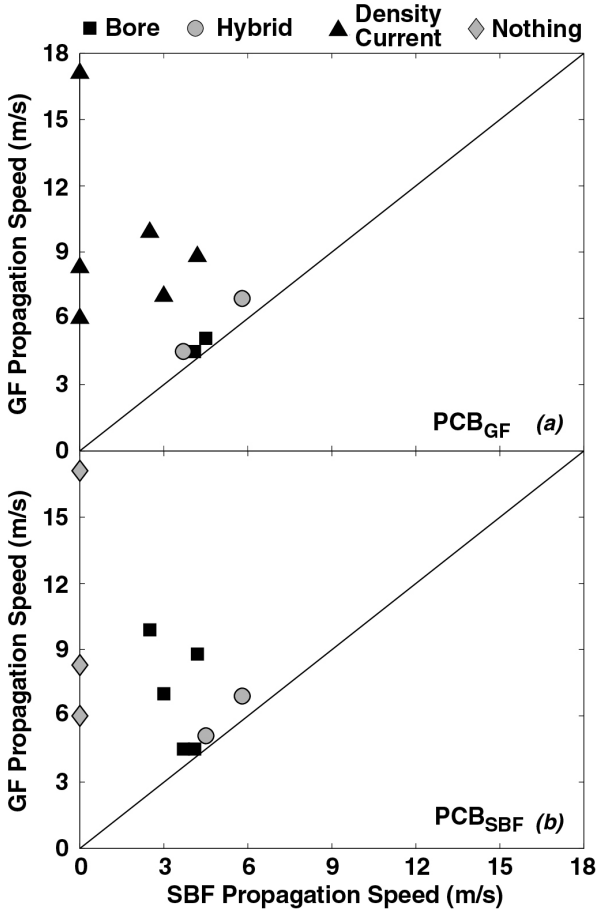

Figure 3. Gust front propagation speed versus sea-breeze front propagation speed for the ten boundary collision cases in this study. Character of resulting (a) gust front induced post-collision boundary and (b) sea-breeze front induced post-collision boundary is coded by the shape and shading of plot symbols (bore: black square, density current: black triangle, hybrid bore/density current: gray circle, no post-collision boundary: gray diamond). Solid line indicates that part of the parameter space where gust front and sea-breeze front propagation speeds are equal.